Structured Reduced Graphene Oxide/Polymer Composites for Ultra-Efficient Electromagnetic Interference Shielding

*Ding-Xiang Yan, Huan Pang, Bo Li, Robert Vajtai, Ling Xu, Peng-Gang Ren, Jian-Hua Wang, and Zhong-Ming Li**

A high-performance electromagnetic interference shielding composite based on reduced graphene oxide (rGO) and polystyrene (PS) is realized via high-pressure solid-phase compression molding. Superior shielding effectiveness of 45.1 dB, the highest value among rGO based polymer composite, is achieved with only 3.47 vol% rGO loading owning to multi-facet segregated architecture with rGO selectively located on the boundaries among PS multi-facets. This special architecture not only provides many interfaces to absorb the electromagnetic waves, but also dramatically reduces the loading of rGO by confining the rGO at the interfaces. Moreover, the mechanical strength of the segregated composite is dramatically enhanced using high pressure at 350 MPa, overcoming the major disadvantage of the composite made by conventional-pressure (5 MPa). The composite prepared by the higher pressure shows 94% and 40% increment in compressive strength and compressive modulus, respectively. These results demonstrate a promising method to fabricate an economical, robust, and highly efficient EMI shielding material.

1. Introduction

An electromagnetic interference shielding effectiveness (EMI SE) value of at least 20 dB is typically required for conductive polymer composite (CPC) materials to be commercially applicable in EMI shielding devices. Reaching this effectiveness typically requires a volume electrical conductivity of at least 1 S m^{-1}.[1] Such high conductivity can be realized through superior conductive interconnected networks, which is achieved with a nanofiller concentration far above the electrical percolation threshold of the composite.[2–4] Even though in case of highly conductive, atomically thin graphene filler been used, an extremely high graphene loading is required. For example, the first graphene based EMI shielding composite exhibited an EMI SE of ≈21 dB with a graphene loading of 15 wt%.[5] Ling et al. reduced the graphene loading of a polyetherimide/graphene composite to 10 wt%, while keeping EMI SE at 20.0 dB.[6] On the other hand, an improved EMI SE, 29.3 dB, of graphene/polystyrene (PS) composite was obtained at the cost of extremely high graphene loading of 30 wt%.[7] Graphene or reduced graphene oxide (rGO) composites based on poly (methyl methacrylate),[8] water-borne polyurethane,[9] phenolic[10] were also reported in published papers, nevertheless, satisfactory EMI SE always requires abundant nanofillers due to the homogenous dispersion structure of these composites. High nanofiller concentrations result in high production costs and poor composite processability. Preparing CPC materials with superior EMI SE at low nanofiller loading remains a challenge.

The formation of segregated architectures can reduce the electrical percolation threshold, and improve electrical conductivity.[11–15] In such architectures, electrical nanofillers are distributed only at the interfaces of polymer granules not homogeneously distributed in the whole volume of the polymer matrix. Graphene was first utilized to construct segregated conductive networks in ultrahigh molecular weight polyethylene (UHMWPE) matrix, exhibiting an electrical conductivity of 0.04 S m^{-1} at a rather low content of 0.6 vol%.[12] A comparative study of segregated and homogeneous graphene/polycarbonate composites showed that the percolation threshold of the former composite was one third of that for the latter, and electrical conductivity was also higher by 220% at the same graphene loading of 4 wt%.[13] Segregated architectures also provide enhanced EMI SE, for example, when Cu nanowires were used as an electrical nanofiller in PS, the segregated composites exhibited EMI SE levels of 26 and 42 dB at 10 and 13 wt% Cu loading, respectively.[15] Very recently, our group reported an in situ thermally reduced graphene/ultrahigh molecular weight polyethylene composite with a segregated structure, revealing the EMI SE of 28.3–32.4 dB at an ultralow graphene loading.[16] Although the formation of such segregated architectures could improve electrical and EMI shielding performance, one major issue of segregated architectures is that the existence of nanofiller agglomerates at polymer granule interfaces restricts molecular diffusion between granules, leading to poor

Dr. D.-X. Yan, H. Pang, L. Xu, Prof. P.-G. Ren, Prof. Z.-M. Li
College of Polymer Science and Engineering
State Key Laboratory of Polymer Materials Engineering
Sichuan University
Chengdu 610065, P. R. China
E-mail: zmli@scu.edu.cn
Dr. B. Li, Dr. R. Vajtai
Department of Materials Science and NanoEngineering
Rice University
Houston, Texas 77005, USA
Prof. J.-H. Wang
Institute of Chemical Materials, Chinese Academy of Engineering Physics
Mianyang 621900, P. R. China

DOI: 10.1002/adfm.201403809

mechanical performance of the segregated materials and limitation in application.[17]

In the current study, the rGO/PS EMI shielding composite with superior EMI SE, low active materials loading and enhanced mechanical performance has been realized through a combination of segregated architecture and high-pressure solid-phase compression molding at 350 MPa. The high-pressure molded segregated composite with only 3.47 vol% rGO exhibits an average EMI SE of 45.1 dB, which is the highest reported EMI SE for graphene-based polymer composites to the best of our knowledge. The composite exhibits the excellent compressive strength and modulus of 108.4 MPa and 2.75 GPa, respectively, showing 94% and 40% increase compared to the reference sample obtained through the conventional-pressure molding. In addition, a comprehensive study of the fundamental shielding mechanism, the influence of sample thickness and polymer particle size, has been performed.

2. Results and Discussion

The fabrication process is shown schematically in **Figure 1**a–d. First, GO (orange flake) was dispersed in distilled water (1 mg/mL) by stirring and ultrasonication (400 W, 40 kHz) to create a homogeneous dispersion, and the desired quantity of PS particles (blue spheres) was added under vigorous stirring for another 30 min (Figure 1a). An in situ reduction was carried out to convert GO to rGO (black flake) with hydrazine hydrate at 95 °C for 3 h (Figure 1b). The product was collected by filtration and dried in a vacuum oven at 80 °C for 6 h to remove residual solvent, and the rGO-coated PS complex particles were ultimately compression molded into sheets with various thicknesses by subjecting to 350 MPa at 100 °C for 10 min (Figure 1c). This yielded s-rGO/PS composites with various rGO content (Figure 1d), and PS particles deformed into multi-facets with rGO conductive layers sandwiched among contacting interfaces and joints. The processing temperature (100 °C) was around the glass transition temperature (T_g) of PS, thus the PS composite processing is considered as a solid-phase compression molding.[18]

Though the typical thickness of the sample is selected in the range of millmeters to to provide high EMI SE, this technique can be applied for the fabrication of flexible s-rGO/PS thin film with a thickness as low as 20 μm, suggesting the potential in flexible and wearable applications (Figure 1e).[19] Figure 1f shows the optical microscopy image of the film (5 μm) cut from the s-rGO/PS composite containing 0.14 vol% rGO, providing insight into its structural formation. The transmission light mode was used. The distribution of rGO in the s-rGO/PS composite can be easily identified due to the light transmittance difference between rGO and PS, that is, the rGO enriched region appears to be dark and the rGO scarce region appears to be bright. As observed, the rGO enriched region segregates the rGO scarce region distinctly, which confirms that rGO is selectively distributed at the interfaces of PS multi-facets, forming interconnected networks throughout the composite. As the processing temperature is around the T_g of PS, suggesting a solid-phase compression molding. Though the PS molecular chain segments can motion at this temperature, the movement of PS long molecular chains are confined, which would prevent the rGO from penetrating into PS regions, and ensure the selective distribution of rGO. PS multi-facets that rGO failed to penetrate into are regarded as "excluded volume", which increases the effective rGO concentration and the probability of forming more conducting pathways.[13] The high resolution TEM image at the interface between two PS multi-facets (Figure 1g) shows an interface with densely packed rGO. Some rGO flakes can be found penetrating into the surface of PS multi-facets, though not deep inside. The dense rGO regions

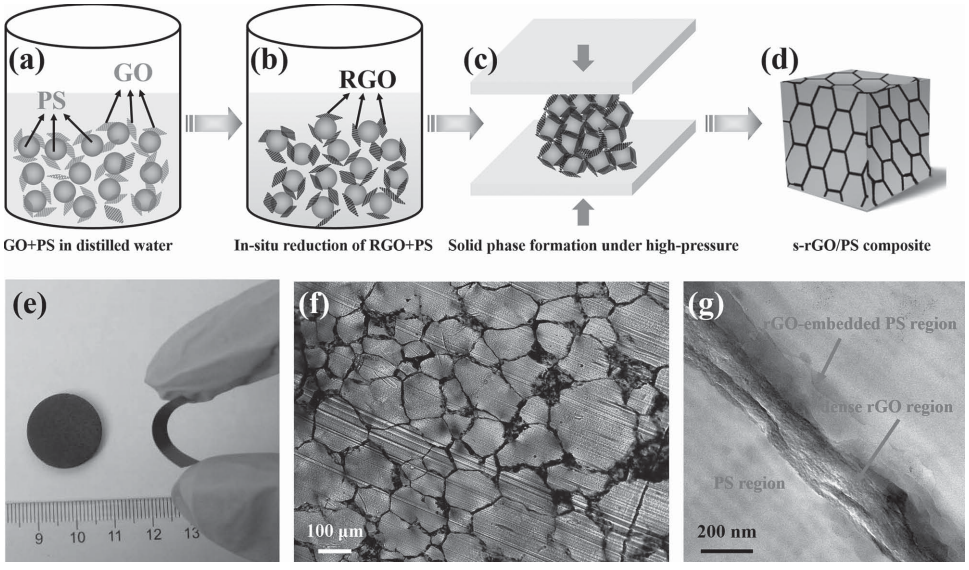

Figure 1. Schematic of the fabrication of the segregated rGO/PS (s-rGO/PS) composite under high pressure: a) Steps of the method shown are suspended GO and PS particles in distilled water; b) in situ reduction of the GO/PS mixture in the presence of hydrazine hydrate; c) obtained rGO/PS powder after the removal of water; d) resulting s-rGO/PS composite; e) optical photograph of the flexible s-rGO/PS thin film (20 μm in thickness) and the sample for EMI SE measurement; f) cross-sectional optical microscopy image of the s-rGO/PS composite containing 0.14 vol%rGO; g) TEM image of rGO layers between PS regions.

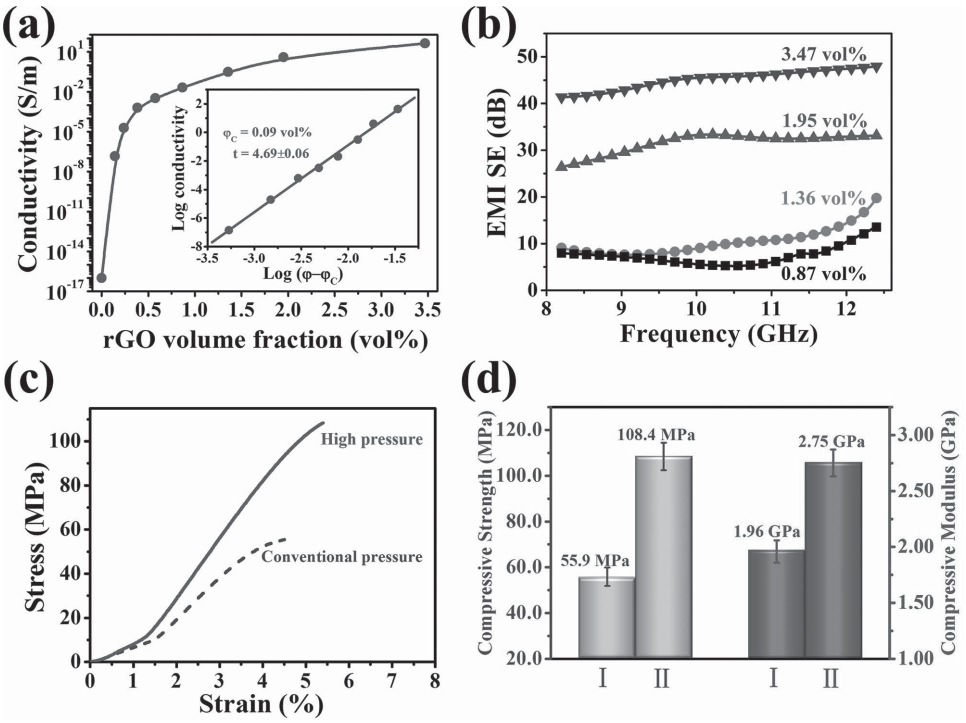

Figure 2. a) Electrical conductivity versus rGO loading for the s-rGO/PS composites; b) EMI SE as a function of frequency in X-band range for the composites; c) typical stress-strain curves of the s-rGO/PS composites with 1.95 vol% rGO molded under high and conventional pressure; and d) compressive strength and modulus of the s-rGO/PS composites. I and II indicate composites molded under conventional and high pressure, respectively.

containing the major portion of rGO between adjacent PS multi-facets form highly conductive network leading to enhanced electrical conductivity. The formation of rGO-embedded PS region containing a discernible amount of rGO illustrates the intensive diffusion of PS chains into/across rGO layer at such a high pressure (350 MPa). The enhanced the interfacial interaction between rGO and the PS matrix would lead to improved mechanical properties of the composite.

The dependence of electrical conductivity of the s-rGO/PS composite on rGO loading is shown in **Figure 2**a. The dimension of the testing sample is 15 (length) × 10 (width) × 2.5 (thickness) mm^3, unless mentioned otherwise. An increase of nearly 10 orders of magnitude is observed for conductivity, upon increasing the rGO content from 0 to 0.14 vol%, demonstrating typical percolation behavior. Similar to the segregated Cu nanowire/PS composites,[15] the power-law equation is used here to evaluate the relationship between electrical conductivity and rGO concentration, where σ is the electrical conductivity of the composite, σ_0 is a constant related to the intrinsic conductivity of rGO, φ is the volume fraction of rGO, φ_C is the percolation threshold, and t is a critical exponent dependent on the electrical network mechanism.[20] The inset in Figure 2a shows the best fit result using the power law equation. φ_C is found to be 0.09 vol%, which is among the lowest threshold values in reported references for rGO-based polymer composites.[21–24] This low threshold value can be attributed to the large rGO aspect ratio, and the dense conducting rGO region formed around PS multi-facets at high pressure. The fitted value of t is 4.69, much higher than the universal critical exponents (1.1–2.0) derived from the classical conduction model.[25] The microstructural properties (wrinkled surface, extreme geometry, large aspect ratio) of rGO are thought to be responsible for the high critical exponent.[26–28] A conductivity of 43.5 S m^{-1} is achieved at a rGO loading of 3.47 vol%, which exceeds the target conductivity (1 S m^{-1}) for EMI shielding applications.[1] The obtained conductivity here is highest among previously reported segregated polymer composite materials using graphene (or graphene derivatives), carbon nanotube, and carbon nanofiber.[29–34]

Figure 2b shows the EMI SE of the s-rGO/PS composites in the X-band (8.2–12.4 GHz). Schematic of measurement setup is shown in Figure S4 in Supporting Information. EMI SE exhibits weak frequency dependence across the measured frequency range, which allows the average EMI SE to be used to evaluate the EMI shielding effect. EMI SE is closely related to the rGO loading. For example, the average EMI SE of a 1.36 vol% rGO composite is 10.3 dB, indicating that ≈90% of the electromagnetic radiation is blocked by the shielding material (EMI SE is defined as the logarithmic ratio of incident to transmitted power). As the rGO loading rises to 1.95 and 3.47 vol%, the EMI SE increases to 31.5 and 45.1 dB, respectively, which indicates 0.07 and 0.003% transmission through the shielding material. The increased EMI SE is attributed mainly to the increased conductivity of the s-rGO/PS composite at higher rGO loading.[15] Additionally, the thickness and continuity of the rGO conductive network also influence the EMI SE of the composites. A higher rGO concentration results in a thicker conductive interface between PS multi-facets leading to stronger interaction with incoming electromagnetic waves, improving the shielding effectiveness.

In addition to excellent electrical and EMI SE properties, favorable mechanical properties are also demanded for a practical EMI shielding material. Conventional solid-state mixing and latex technology are effective methods for achieving segregated polymer composites with good electrical conductivity or EMI shielding properties.[14–16,23,35] However, the resultant composites consistently exhibit poor mechanical properties due to the weak adhesive interaction between the pristine nanofiller regions and polymer regions.[16] In the current work, both EMI shielding and favorable mechanical performance are enhanced dramatically by the high-pressure compression molding of the s-rGO/PS composite. Mechanical properties of the high-pressure molded composite and those of a composite molded under conventional pressure are shown in Figure 2c,d. A typical compressive strain-stress test (Figure 2c) illustrates superior compressive performance of high-pressure molded composite (blue solid line) compared to the conventional compression molded composite (black dash line). Figure 2d summarizes the average compressive strength and modulus of both composites. The high-pressure molded composite exhibits an excellent compressive strength (108 MPa) and modulus (2.75 GPa), showing 94% and 40% increase compared to the reference samples obtained through the conventional-pressure molding (55.9 MPa and 1.96 GPa). The enhanced mechanical properties through the high-pressure compressive molding can be attributed to inter-diffusion of PS chains under high pressure across the boundaries between contacting PS multi-facets and at the interfaces among PS and rGO flakes (evidenced by the embedded rGO in PS regions in Figure 1g.

The EMI SE of the s-rGO/PS composites in current work has been greatly improved compared to previously reported rGO-based CPC materials, at similar sample thicknesses and similar or even lower rGO loadings, as listed in **Table 1**. Zhang et al. reported an EMI SE value of ≈30 dB, for a solution-blended rGO/PMMA composite at 8.0 wt% rGO loading.[8] Hsiao et al. reported the use of a cationic surfactant to improve rGO dispersion in water-borne polyurethane, which increased the EMI SE from 18 dB for pristine rGO to 32 dB for cationic surfactant adsorbed rGO, at rGO loading of 7.7 wt%.[9] For the s-rGO/PS composite, the major portion of rGO is distributed at the interfaces of PS multi-facets, instead of being uniformly distributed throughout the whole PS matrix. This localized distribution can greatly enhance the utilization ratio of rGO, leading to reduced rGO loading and increased electrical conductivity of the composite. More importantly, the densely packed graphene-graphene networks at the interfaces can effectively interact with incident radiation leading to the very high EMI SE of 45.1 dB.

Table 1. Average EMI SE in the X-band frequency range, for the s-rGO/PS composites and reported graphene-based CPC materials. The s-rGO/PS composites exhibit higher EMI SE at similar thicknesses and lower rGO loadings. The weight concentrations of rGO are used for comparison.

Polymer	rGO concentration [wt%]	Sample thickness [mm]	EMI SE [dB]	Ref.
PS	7.0	2.5	45.1	Present work
PS	4.0	2.5	31.5	Present work
Epoxy	15.0	2.0	21.0	[5]
PEI[a)]	10.0	2.3	20.0	[6]
PMMA[a)]	5.0	3.4	25.0	[8]
PMMA[a)]	8.0	3.4	30.0	[8]
WPU[a)]	7.7	2.0	18.0 or 32.0	[9]
Phenolic	70	0.3	43.4	[10]
PS	10.0	2.8	18	[36]
PS	1.5 (plus 2.0 CNTs)	5.6	20.2	[37]
PS foam	30.0	2.5	29	[7]
PMMA foam	5.0	2.4	19	[38]
PEI foam	5.0 (plus 5.0 Fe_3O_4)	2.5	17.8	[39]

[a)]PEI, PMMA, and WPU are polyetherimide, poly (methyl methacrylate), and water-borne polyurethane, respectively.

To clarify the EMI shielding mechanism in the s-rGO/PS composites, the total EMI shielding effectiveness (SE_{Total}), microwave absorption (SE_A), and microwave reflection (SE_R) at the frequency of 8.2 GHz were calculated from the measured scattering parameters (detailed calculations are shown in the Supporting Information), and their dependences on rGO loading are plot in **Figure 3**a. It is clear that increasing rGO loading increases both SE_A and SE_R, but the contribution of SE_R is negligible over all the rGO contents. For instance, the SE_{Total}, SE_A, SE_R of the composite with 3.47 vol% rGO are 41.4, 38.4, and 3.0 dB, respectively, which indicates that the contribution of absorption to the total EMI SE (93%) is much larger than that from reflection (7%), suggesting an absorption dominated shielding mechanism. To better understand the absorption-dominated shielding mechanism, the s-rGO/PS composite can be considered as a "skin" composed of closely packed cells, with dense rGO layers as highly conductive "membranes". As shown schematically in Figure 3b, incident electromagnetic microwaves entering the "skin" are attenuated by reflecting, scattering and adsorption many times by the multiple layers of membranes. The cells (PS multi-facets) leads to a great number of membranes such that it is very difficult for waves to penetrate this functional skin. A similar shielding mechanism has been reported for graphene/polymer foam and ordered mesoporous carbon/fused silica composites.[40,41]

To further elucidate the structure-property relation of s-rGO/PS composites, the effect of "skin thickness" on EMI SE of the composites with 3.47 vol% rGO was investigated, as shown in Figure 3c. A significant increase of EMI SE can be found from 15.2 to 41.4 dB at 8.2 GHz and 12.9 to 48.0 dB at 12.4 GHz when the sample thickness increases from 1 to 2.5 mm, due to higher amount of conductive filler that interact with the incoming electromagnetic wave. The composites with the thickness of 1.0 and 1.5 mm own the average EMI SE of 15.0 and 22.2 dB, respectively, and thus the critical thickness when the s-rGO/PS composites starts to show shielding properties (exceed 20 dB) should be between 1.5 to 2.0 mm.[1] A detailed analysis of the contributions of SE_A and SE_R to the SE_{Total} at 8.2 GHz as a function of sample thickness in Figure 3d further demonstrates the adsorption dominated shielding mechanism intensively. It is clearly that SE_A increases with sample thickness while SE_R is almost a constant. The increased EMI SE is primarily contributed by the increase of SE_A. This experiment further suggests that the reflection might only happen at the incident surface of sample. The stacking architecture of multifaceted cells and

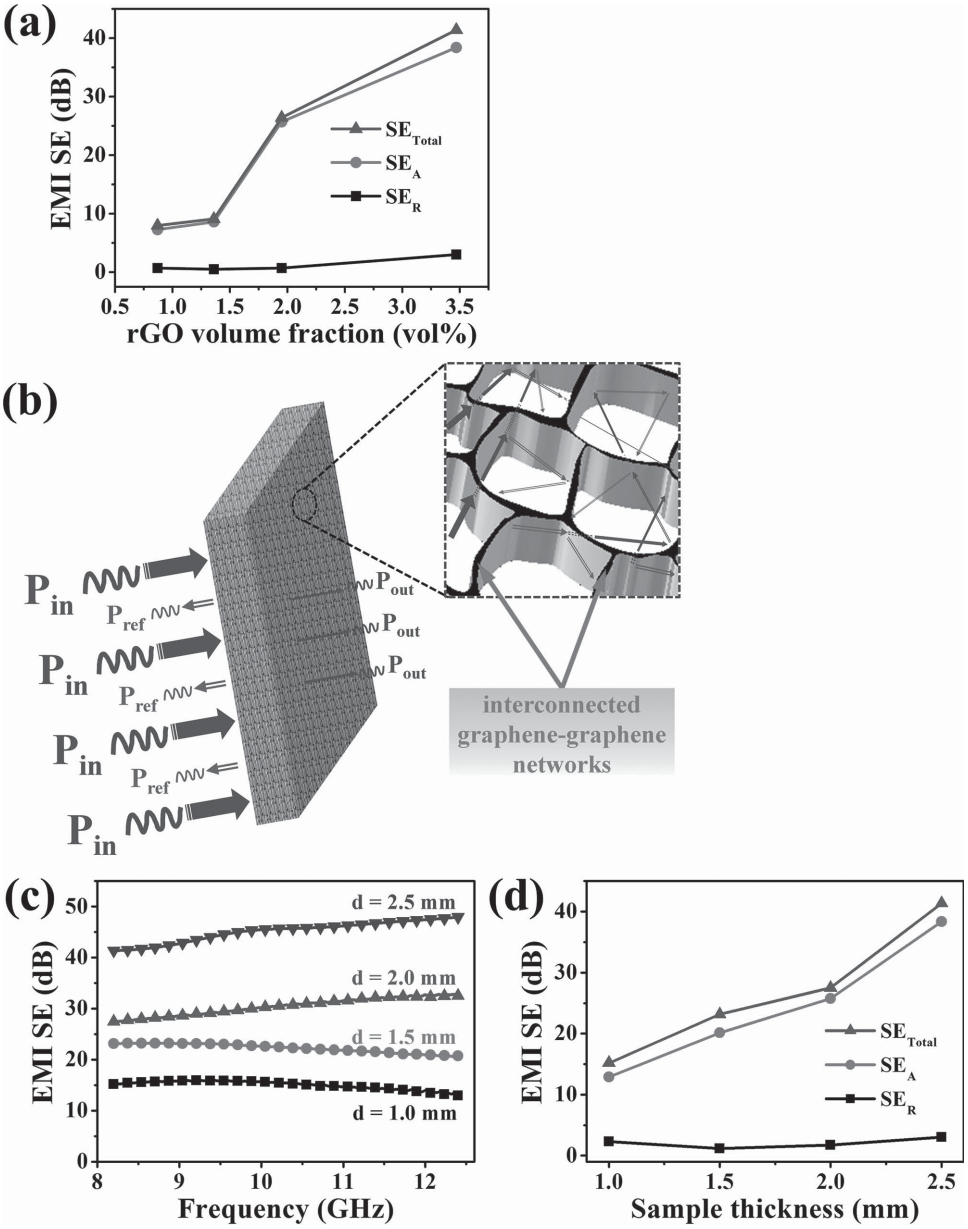

Figure 3. a) Comparison of total EMI shielding effectiveness (SE_{Total}), microwave absorption (SE_A), and microwave reflection (SE_R) at the frequency of 8.2 GHz for the s-rGO/PS composites with various rGO loadings; b) **s**chematic representation of microwave transfer across the s-rGO/PS composite; c) EMI SE as a function of frequency for the composites with various sample thicknesses and the pristine PS with thickness of 2.5 mm, and d) the comparison of SE_{Total}, SE_A, and SE_R as the frequency of 8.2 GHz.

the strong adsorption of rGO membranes keep the wave penetrating the surface inside the "skin" until adequately adsorbed with only trivial amount of energy go through the skin.

Additionally, it is interesting to note that reducing the size of PS particles does not increase the EMI SE. On the contrary, the EMI SE of the composites (with the same rGO loading of 3.47 vol%) increases with the increase of particles diameter from 600 nm to 96 μm, as shown in **Figure 4**a. This is different from the common sense where reducing the particles size might lead to more rGO "membranes" that attenuate the incident electromagnetic microwaves more efficiently by reflecting, scattering and adsorption many times, which should be beneficial to achieve higher EMI SE. The proposition can be tenable assuming that the rGO "membranes" remain original thickness or continuity, as the particle size reduced. Nevertheless, since the rGO content is consistent (3.47 vol%), reducing PS particle size would also result in thinner or discontinuous rGO "membranes" due to the increased surface area of PS particles. Thus a less continuity of the rGO conductive network and less segregated architecture formed with the smaller PS particles,[42] leading to lower electrical conductivity and EMI SE. For instance, the s-rGO/PS composite with the PS particle diameter of 600 nm shows an electrical conductivity of 0.02 S m^{-1}, much lower than those

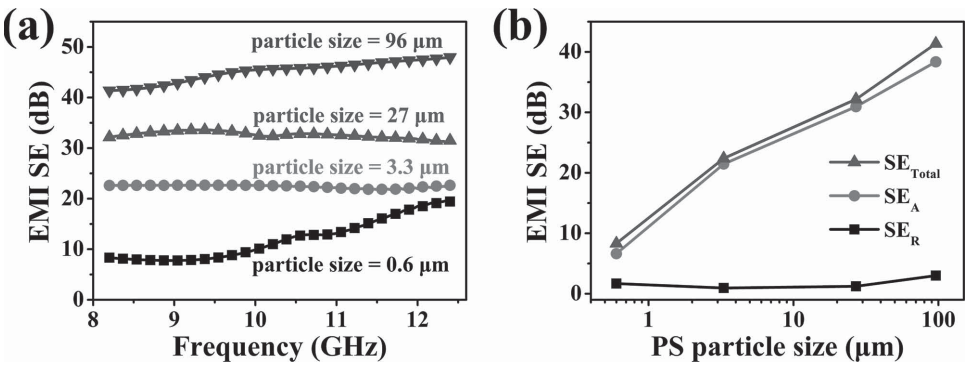

Figure 4. a) EMI SE as a function of frequency for the s-rGO/PS composites with various PS particle size, and b) the comparison of SE_{Total}, SE_A, and SE_R as the frequency of 8.2 GHz.

samples with larger particle diameters of 3.3 μm (1.8 S m^{-1}), 27 μm (32.6 S m^{-1}) and 96 μm (43.5 S m^{-1}). Correspondingly, the average EMI SE for the composite with the smallest PS particle size is only 12.0 dB, even below the target EMI SE value of 20 dB. Therefore, the creating of continuous and densely packed the conductive rGO network becomes the predominant effect here and larger polymer particles size leading to better conductive network is preferred. Figure 4b shows the plots of SE_{Total}, SE_A, SE_R as a function of PS particle size at the frequency of 8.2 GHz. Again, the ca. SE_A/SE_{Total} are 80%, 96%, 96% and 92%, for samples with particle size of 600 nm, 3.3 μm, 27 μm and 96 μm, respectively, confirming that regardless the PS particle size, absorption is the primary shielding mechanism rather than reflection in the s-rGO/PS composites, endorsing again the proposed model in Figure 3b.

As we known, the processing temperature (100 °C) for the s-rGO/PS composite is around the T_g of PS, suggesting a solid-phase compression molding. To further embody the superiority of solid-phase compression molding, the dependence of EMI shielding and compressive performance of the s-rGO/PS composites on processing temperature was examined, as shown in **Table 2**. The EMI SE of the rGO/PS composite prepared at 60 °C is comparable to that of s-rGO/PS composite prepared at 100 °C, nevertheless, the compressive strength and modulus are seriously deteriorated. Below T_g, the PS molecular chains are frozen, and only atoms or groups can vibrate near their equilibrium position. At this processing temperature, the rGO was difficult to penetrate into the PS multi-facets and the composite presented comparable EMI SE. However, though a high pressure of 350 MPa was applied, the relatively poor interfacial adhesion between PS multi-facets still existed in the composite due to the extremely weak movement of PS molecular chain segments, which undoubtedly resulted in reduced mechanical properties. As the temperature increases to 180 °C, which is much higher than T_g, though the compressive properties of the composite rise to some extent, the corresponding EMI SE decreases remarkably. At such a high temperature, the melt viscosity of PS obviously dropt and the rGO easily diffused into PS multi-facets. Accordingly the effective rGO concentration to form conducting pathways in the composite significantly reduced, leading to reduced EMI SE.

Finally, we performed the effect of compression pressure (5, 100, 200, 350 MPa) on the EMI shielding and compressive performance of the s-rGO/PS composite to embody the superiority of high pressure, as shown in **Table 3**. It can be seen that the average EMI SE of the rGO/PS composites varies from 30.6 to 31.5 dB with the compression pressure ranging from 5 to 350 MPa, exhibiting a very weak compression pressure dependence. The EMI shielding performance of the rGO/PS composite is mainly related to the thickness and continuity of the rGO conductive network (characterized by electrical conductivity). As the processing temperature (100 °C) is around the T_g of PS, suggesting a solid-phase compression molding, the PS molecular chain segments can motion while the movement of long PS chains are confined. Though the introduction of high pressure (350 MPa) would result in inter-diffusion of PS chains at the interfaces among PS and rGO and thus the penetration of some rGO nanosheets into the surface of PS multi-facets (shown in Figure 1g), the major portion of rGO nanosheets are still selectively distributed between adjacent PS multi-facets to form dense rGO conductive network, exhibiting similar thickness and continuity of the rGO conductive network to that of

Table 2. The effect of processing temperature on EMI shielding and compressive performance of the rGO/PS composites loaded with 1.95 vol% rGO.

Processing temperature [°C]	Average EMI SE [dB]	Compressive strength [MPa]	Compressive modulus [GPa]
60	29.3	43.3	2.12
100	31.5	108.4	2.75
180	21.0	99.2	2.64

Table 3. The effect of compression pressure on EMI shielding and compressive performance of the rGO/PS composites loaded with 1.95 vol% rGO. The processing temperature is fixed at 100 °C.

Compression pressure [MPa]	Average EMI SE [dB]	Compressive strength [MPa]	Compressive modulus [GPa]
5	31.1	55.9	1.96
100	30.6	71.5	2.04
200	31.2	81.6	2.42
350	31.5	108.4	2.75

conventional-pressure molded composite. As a consequence, the electrical conductivities and EMI SE of the composites varies slightly from 3.2 to 4.5 S m^{-1} across the pressure range (5 to 350 MPa). However, with the increase of compression pressure, compressive strength and modulus of the composite substantially rise. Compared to the composite molded at 5 MPa, the composites molded at 100, 200, 350 MPa exhibit 28%, 46%, 94% increase in compressive strength, and 4%, 23%, 40% increase in compressive modulus. The enhanced mechanical properties with the increase of compression pressure can be attributed to inter-diffusion of PS chains across the boundaries between contacting PS multi-facets and at the interfaces among PS and rGO layers. At the present stage, we are not able to further increase the compression pressure beyond 350 MPa due to the melt leakage of the mold, and thus the optimal pressure of 350 MPa was chosen in this work. On the basis of these results, one can design desirable EMI shielding s-rGO/PS composites with tunable mechanical properties, meeting the requirement of various environmental conditions.

3. Conclusion

We have integrated a segregated hybrid architecture (PS multi-facets as cells and rGO conductive layers as membranes) with high-pressure solid-phase compression molding (350 MPa) to create a highly efficient EMI shielding materials with low active material loading (0.09 vol%) and superior mechanical properties. The composite shows significant improvements in compressive strength (94%) and compressive modulus (40%) compared to that made by conventional low pressure molding. The average EMI SE of the segregated composite containing only 3.47 vol% rGO achieves 45.1 dB, and is the highest reported value for graphene-based polymer composites. The segregated architecture provides numerous reflecting and adsorption conductive interfaces (rGO conductive layers) leading to excellent EMI SE, and an absorption-dominated shielding mechanism. Our method could pave the way to the fabrication of cheap, robust and highly efficient EMI shielding or electromagnetic absorption materials.

4. Experimental Section

Materials: Graphene oxide (GO) was synthesized from expanded graphite by the modified Hummers method, as described in our previous work.[7] The typical atomic force microscopy images of GO are shown in Figure S1 in Supporting Information. The GO exhibited a thickness of 1–2 nm and average particle size of 0.87 μm. The aspect ratio of GO was estimated to be 453-870. The particle size distribution of GO counted from Figure S1 is shown in Figure S2. PS was a commercial polymer (GP5250, average $M_w \approx 233\,000$, $M_w/M_n = 1.78$) kindly supplied by Formosa Chemicals & Fiber Corporation, Taiwan. Three kinds of PS particles were used in this work with the average particle size of 96, 27, and 0.6 μm (The size distributions of PS particles were shown in Figure S3 in the Supporting Information.). H_2SO_4, $KMnO_4$, H_2O_2, HCl and hydrazine hydrate were all analytical grade and supplied by Chengdu Kelong Chemical Reagent Factory (Chengdu, China).

Characterizations: For optical microscopy observations, 5-μm-thick specimens were prepared by a microtome, and observed with an Olympus BX51 polarizing optical microscope (Olympus Co., Tokyo, Japan) equipped with a MicroPublisher 3.3 RTV CCD camera. Fifty to sixty nanometer-thick composite thin films were prepared for transmission electron microscopy (TEM) observation by a Leica EMUC6/FC6 microtome, and observed using a FEI Tecnai F20 instrument at 200 kV. For electrical resistivity measurements, a Keithley electrometer model 4200CSC (USA) and a four-point probe instrument (SDY-6, Guangzhou, China) were used to measure the resistivity. EMI shielding characteristics of the s-rGO/PS composite reported here were made by us using a coaxial test cell (APC-7 connector) in conjunction with an Agilent N5230 vector network analyzer, according to ASTM ES7-83 (Schematic of measurement setup was shown in Figure S4 in Supporting Information.). The APC-7 connector is a precision coaxial connector that was used on laboratory microwave test equipment and can be utilized at frequencies up to 18 GHz. The Agilent N5230 vector network analyzer was calibrated using the standard APC-7 connector open, short, and 50 Ω loads. The intermediate frequency bandwidth was set as 1 kHz during the measurement and 201 points were collected for each specimen. Thus the frequency dependence of shielding effectiveness in the frequency range of 8.2–12.4 GHz (X-Band) obtained here is accurate and reliable. Samples 10 mm in diameters with various thicknesses were placed in the specimen holder, which were connected through Agilent 85132F coaxial line to separate VNA ports. The scattering parameters (S_{11} and S_{21}) of the s-rGO/PS composites in the frequency range of 8.2–12.4 GHz (X-Band) were gained to calculate the EMI SE. EMI SE (SE_{Total}) is the summation of the reflection from the material surface (SE_R), the absorption of electromagnetic energy (SE_A), and the multiple internal reflections (SE_M) of electromagnetic radiation. SE_R is related to the impedance mismatch between air and absorber; SE_A can be regarded as the energy dissipation of the electromagnetic microwave in the absorber; and SE_M is considered as the scattering effect of the inhomogeneity within the materials which can be negligible when $SE_{Total} \geq 15$ dB. The detailed calculations of SE_R, SE_A, and SE_M is shown in Supporting Information. The compressive strength and compressive modulus were measured with a universal electronic tensile machine (Shimadzu, Japan), with a compression rate of 2 mm/min on samples 16 mm in diameter and 40 mm in thickness.

Supporting Information

Supporting Information is available from the Wiley Online Library or from the author.

Acknowledgements

The authors gratefully acknowledge financial support from the National Natural Science Foundation of China (No. 51120135002, 51121001). This project was also funded by the Chinese Academy of Engineering Physics and Sichuan University Collaborative Innovation Fund (No. XTCX2011003). B.L. and R.V. would like to acknowledge the support by the U.S. Air Force Office of Scientific Research MURI grant FA9550-12-1-0035.

Received: October 29, 2014
Revised: November 13, 2014
Published online: December 2, 2014

[1] J. M. Thomassin, C. Jérôme, T. Pardoen, C. Bailly, I. Huynen, C. Detrembleur, *Mater. Sci. Eng., R* **2013**, *74*, 211.
[2] Z. Chen, W. Ren, L. Gao, B. Liu, S. Pei, H.-M. Cheng, *Nat. Mater.* **2011**, *10*, 424.
[3] X. Gui, H. Li, L. Zhang, Y. Jia, L. Liu, Z. Li, J. Wei, K. Wang, H. Zhu, Z. Tang, *ACS Nano* **2011**, *5*, 4276.
[4] X. Sun, H. Sun, H. Li, H. Peng, *Adv. Mater.* **2013**, *25*, 5153.

[5] J. J. Liang, Y. Wang, Y. Huang, Y. F. Ma, Z. F. Liu, J. M. Cai, C. D. Zhang, H. J. Gao, Y. S. Chen, *Carbon* **2009**, *47*, 922.
[6] J. Ling, W. Zhai, W. Feng, B. Shen, J. Zhang, W. Zheng, *ACS Appl. Mater. Interfaces* **2013**, *5*, 2677.
[7] D. X. Yan, P. G. Ren, H. Pang, Q. Fu, M. B. Yang, Z. M. Li, *J. Mater. Chem.* **2012**, *22*, 18772.
[8] H. B. Zhang, W. G. Zheng, Q. Yan, Z. G. Jiang, Z. Z. Yu, *Carbon* **2012**, *50*, 5117.
[9] S. T. Hsiao, C. C. M. Ma, H. W. Tien, W. H. Liao, Y. S. Wang, S. M. Li, Y. C. Huang, *Carbon* **2013**, *60*, 57.
[10] A. P. Singh, P. Garg, F. Alam, K. Singh, R. Mathur, R. Tandon, A. Chandra, S. Dhawan, *Carbon* **2012**, *50*, 3868.
[11] A. V. Kyrylyuk, M. C. Hermant, T. Schilling, B. Klumperman, C. E. Koning, P. van der Schoot, *Nat. Nanotechnol.* **2011**, *6*, 364.
[12] H. Pang, T. Chen, G. M. Zhang, B. Q. Zeng, Z. M. Li, *Mater. Lett.* **2010**, *64*, 2226.
[13] M. Yoonessi, J. R. Gaier, *ACS Nano* **2010**, *4*, 7211.
[14] Y. Zhan, M. Lavorgna, G. Buonocore, H. Xia, *J. Mater. Chem.* **2012**, *22*, 10464.
[15] G. A. Gelves, M. H. Al-Saleh, U. Sundararaj, *J. Mater. Chem.* **2011**, *21*, 829.
[16] D. X. Yan, H. Pang, L. Xu, Y. Bao, P. G. Ren, J. Lei, Z. M. Li, *Nanotechnology* **2014**, *25*, 145705.
[17] H. Pang, D.-X. Yan, Y. Bao, J.-B. Chen, C. Chen, Z.-M. Li, *J. Mater. Chem.* **2012**, *22*, 23568.
[18] K. M. Kulkarni, *Polym. Eng. Sci.* **1979**, *19*, 474.
[19] R. Kumar Srivastava, T. Narayanan, A. Reena Mary, M. Anantharaman, A. Srivastava, R. Vajtai, P. M. Ajayan, *Appl. Phys. Lett.* **2011**, *99*, 113116.
[20] H. Hu, G. Zhang, L. Xiao, H. Wang, Q. Zhang, Z. Zhao, *Carbon* **2012**, *50*, 4596.
[21] V. H. Pham, T. T. Dang, S. H. Hur, E. J. Kim, J. S. Chung, *ACS Appl. Mater. Interfaces* **2012**, *4*, 2630.
[22] X. Y. Qi, D. Yan, Z. Jiang, Y. K. Cao, Z. Z. Yu, F. Yavari, N. Koratkar, *ACS Appl. Mater. Interfaces* **2011**, *3*, 3130.
[23] C. Wu, X. Huang, G. Wang, L. Lv, G. Chen, G. Li, P. Jiang, *Adv. Funct. Mater.* **2013**, *23*, 506.
[24] S. Stankovich, D. A. Dikin, G. H. B. Dommett, K. M. Kohlhaas, E. J. Zimney, E. A. Stach, R. D. Piner, S. B. T. Nguyen, R. S. Ruoff, *Nature* **2006**, *442*, 282.
[25] M. B. Heaney, *Phys. Rev. B* **1995**, *52*, 12477.
[26] I. Balberg, *Phys. Rev. Lett.* **1987**, *59*, 1305.
[27] N. Li, Y. Huang, F. Du, X. B. He, X. Lin, H. J. Gao, Y. F. Ma, F. F. Li, Y. S. Chen, P. C. Eklund, *Nano Lett.* **2006**, *6*, 1141.
[28] V. H. Pham, T. V. Cuong, T. T. Dang, S. H. Hur, B. S. Kong, E. J. Kim, E. W. Shin, J. S. Chung, *J. Mater. Chem.* **2011**, *21*, 11312.
[29] M. Li, C. Gao, H. Hu, Z. Zhao, *Carbon* **2013**, *65*, 371.
[30] I. Jurewicz, P. Worajittiphon, A. A. K. King, P. J. Sellin, J. L. Keddie, A. B. Dalton, *J. Phys. Chem. B* **2011**, *115*, 6395.
[31] Q. Liu, J. Tu, X. Wang, W. Yu, W. Zheng, Z. Zhao, *Carbon* **2012**, *50*, 339.
[32] G. Long, C. Tang, K. W. Wong, C. Man, M. Fan, W. M. Lau, T. Xu, B. Wang, *Green Chem.* **2013**, *15*, 821.
[33] R. Ou, S. Gupta, C. A. Parker, R. A. Gerhardt, *J. Phys. Chem. B* **2006**, *110*, 22365.
[34] N. K. Shrivastava, B. B. Khatua, *Carbon* **2011**, *49*, 4571.
[35] H. Pang, C. Chen, Y. Bao, J. Chen, X. Ji, J. Lei, Z. M. Li, *Mater. Lett.* **2012**, *79*, 96.
[36] C. Li, G. Yang, H. Deng, K. Wang, Q. Zhang, F. Chen, Q. Fu, *Polym. Int.* **2012**, *62*, 1077.
[37] S. Maiti, N. K. Shrivastava, S. Suin, B. B. Khatua, *ACS Appl. Mater. Interfaces* **2013**, *5*, 4712.
[38] H. B. Zhang, Q. Yan, W. G. Zheng, Z. X. He, Z. Z. Yu, *ACS Appl. Mater. Interfaces* **2011**, *3*, 918.
[39] B. Shen, W. Zhai, M. Tao, J. Ling, W. Zheng, *ACS Appl. Mater. Interfaces* **2013**, *5*, 11383.
[40] Z. Chen, C. Xu, C. Ma, W. Ren, H.-M. Cheng, *Adv. Mater.* **2013**, *25*, 1296.
[41] J. Wang, C. Xiang, Q. Liu, Y. Pan, J. Guo, *Adv. Funct. Mater.* **2008**, *18*, 2995.
[42] G. P. Moriarty, J. H. Whittemore, K. A. Sun, J. W. Rawlins, J. C. Grunlan, *J. Polym. Sci. Part B: Polym. Phys.* **2011**, *49*, 1547.